Inorganic Chemistry

Article

pubs.acs.org/IC

Effects of Linker Torsional Constraints on the Rate of Ground-State Hole Transfer in Porphyrin Dyads

Christopher J. Hondros,[†] Kunche Aravindu,[‡] James R. Diers,[†] Dewey Holten,*[,§] Jonathan S. Lindsey,*[,‡] and David F. Bocian*[,†]

[†]Department of Chemistry, University of California Riverside, Riverside, California 92521-0403, United States

[‡]Department of Chemistry, North Carolina State University, Raleigh, North Carolina 27695-8204, United States

[§]Department of Chemistry, Washington University, St. Louis, Missouri 63130-4889, United States

Supporting Information

ABSTRACT: Understanding hole/electron-transfer processes among interacting constituents of multicomponent molecular architectures is central to the fields of artificial photosynthesis and molecular electronics. Herein, we utilize a recently demonstrated ^{203}Tl/^{205}Tl hyperfine "clocking" strategy to probe the rate of hole/electron transfer in the monocations of a series of three thallium-chelated porphyrin dyads, designated **Tl$_2$-U**, **Tl$_2$-M**, and **Tl$_2$-B**, that are linked via diarylethynes wherein the number of *ortho*-dimethyl substituents on the aryl group of the linker systematically increases (none, one, and two, respectively). Variable-temperature (160−340 K) EPR studies on the monocations of the three dyads were used to examine the thermal activation behavior of the hole/electron-transfer process and reveal the following: (1) Hole/electron transfer at room temperature (295 K) slows as torsional constraints are added to the diarylethyne linker [k(**Tl$_2$-U**) > k(**Tl$_2$-M**) > k(**Tl$_2$-B**)], with rate constants that correspond to time constants in the 2−5 ns regime. (2) As the temperature decreases, the hole/electron-transfer rates for the monocations of the three types of dyads converge and then cross over. At the lowest temperatures examined (160−170 K), the trend in the hole/electron-transfer rates is essentially reversed [k(**Tl$_2$-B**) > k(**Tl$_2$-M**) ∼ k(**Tl$_2$-U**)]. The trends in the temperature dependence of hole/electron-transfer among the three dyads are consistent with torsional motions of the aryl rings of the linker providing for thermal activation of the process at higher temperatures in the case of the less torsionally constrained dyads, **Tl$_2$-U** and **Tl$_2$-M**. In the case of the most torsionally constrained dyad, **Tl$_2$-B**, the hole/electron-transfer process is activationless at all temperatures studied. The reversal in rates of hole/electron transfer among the three dyads at low temperature is qualitatively explained by the results of density functional theory calculations, which predict that static electronic factors could dominate the hole/electron-transfer process when torsional dynamics are thermally diminished.

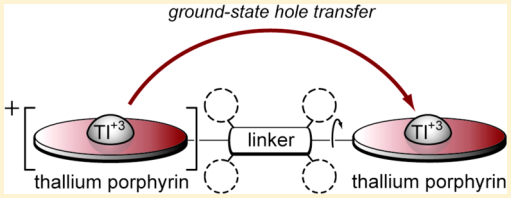

I. INTRODUCTION

Understanding electronic communication among interacting chromophores is essential for the rational design of molecular architectures for artificial photosynthetic light harvesting and energy conversion. Porphyrinic macrocycles have been widely employed in the construction of synthetic light-harvesting arrays owing to their attractive and versatile physical properties and amenability to synthetic control.[1−16] An effective light-harvesting array absorbs intensely and transfers the resulting electronic excited-state energy to a specific site with high efficiency. Conversion of the harvested excited-state energy to electrical energy then requires efficient electron injection into the anode followed by efficient ground-state hole migration away from the anode, thereby preventing charge recombination. Accordingly, understanding hole mobility in prototypical light-harvesting and charge-separation systems is of fundamental interest.

Our groups have previously investigated ground-state hole/electron transfer in oxidized porphyrinic arrays using EPR spectroscopy.[13] This approach entails analysis of the hyperfine interactions observed in the EPR spectrum of the π-cation radical. In early work, the hyperfine interactions due to the naturally abundant ^{1}H and ^{14}N nuclei were used to "clock" the hole/electron-transfer process.[13,17−19] Subsequently, arrays prepared with site-specific ^{13}C labels were employed.[20−22] More recently, we have found that ^{203}Tl/^{205}Tl hyperfine "clocks" are greatly superior to those provided by ^{1}H, ^{14}N, or ^{13}C owing to the fact that the ^{203}Tl/^{205}Tl hyperfine couplings are much larger (15−25 G) than those of the ^{1}H, ^{14}N, or ^{13}C nuclei (1−6 G).[23] The large ^{203}Tl/^{205}Tl hyperfine interactions permit accurate simulations of the EPR spectra of the π-cation radicals of the arrays and the extraction of specific rate constants of hole/electron transfer.

We have applied the ^{203}Tl/^{205}Tl hyperfine-clock strategy to a variety of porphyrin dyads that are joined at a meso position of the porphyrin macrocycle via linkers of a range of lengths and composition (diphenylethyne, diphenylbutadiyne, and (*p*-

Received: July 23, 2012

   dx.doi.org/10.1021/ic301613k | *Inorg. Chem.* XXXX, XXX, XXX−XXX

Chart 1. Thallium(III) Porphyrin Dyads and Corresponding Monomers

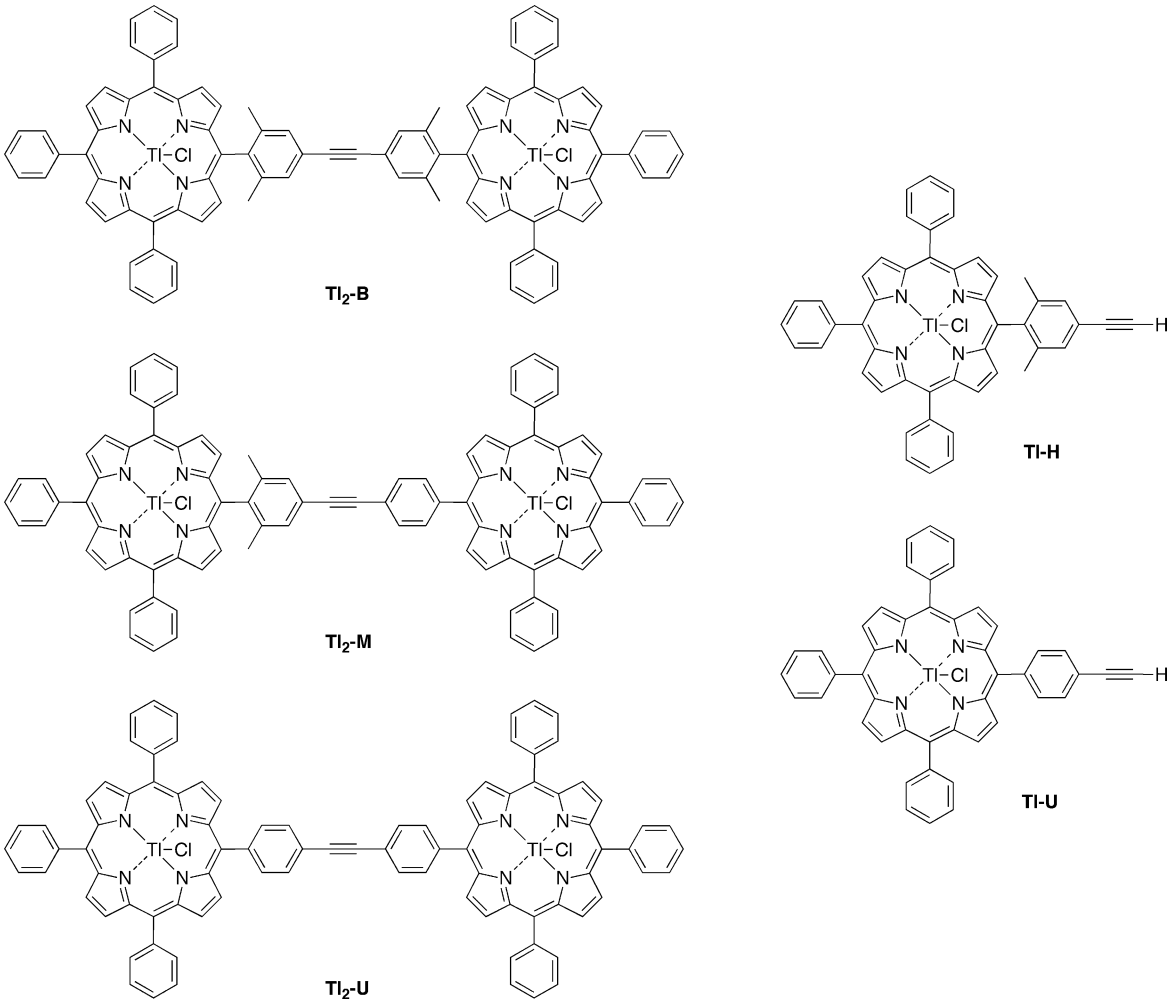

phenylene)$_n$ where n = 1−4).[23] The hole/electron-transfer time constants at room temperature were found to be in the regime of hundreds of picoseconds to subten nanoseconds, depending on the specific porphyrin and/or linker. Variable-temperature EPR studies were used to probe the activation energies of the hole/electron-transfer process. These studies demonstrated that the hole/electron-transfer process is typically weakly activated (12−15 kJ mol^{-1}) from room temperature down to ∼220 K; at temperatures in the 160−220 K range, the process is essentially activationless. However, the detailed characteristics of the activation behavior depend on the nature of the linker. The (*p*-phenylene)$_n$-linked dyads (n = 1−4) are illustrative of this point. The dyad with a single *p*-phenylene linker exhibits weakly activated hole/electron transfer over the 160−295 K temperature range. As the number of *p*-phenylenes in the linker increases, the activation energy monotonically decreases such that the dyad with four *p*-phenylenes in the linker exhibits activationless hole/electron transfer over the full temperature range studied. We have proposed that the activation process for hole/electron transfer in the *p*-phenylene- (and diphenylethyne- and diphenylbutadiyne-) linked dyads is primarily due to restricted torsional motions of the aryl rings of the linker.

The proposal that the activation process for hole/electron transfer in the porphyrin dyads is due to restricted torsional motions of the aryl rings in the linker, while reasonable, has yet to be tested in a systematic fashion. The *p*-phenylene-linked dyads do not provide for such a test because the length of the linker and the energy of the highest-occupied molecular orbital (HOMO) of the linker also vary as the number of *p*-phenylene units increases.[23] These factors, as well as torsional constraints, will contribute to the overall barrier for hole/electron transfer. To minimize the contribution of linker length and HOMO energetics to the hole/electron-transfer process, we report herein the results of studies on a set of thallium porphyrin dyads wherein the only significant difference in the linker is the degree of torsional constraint. These dyads, designated **Tl$_2$-U**, **Tl$_2$-M**, and **Tl$_2$-B**, contain a diarylethyne linker wherein *ortho*-dimethyl substituents are systematically added to the aryl rings of the linker (Chart 1). Two representative monomeric thallium porphyrins, **Tl-U** and **Tl-H**, were also examined (Chart 1).

The rationale for the incorporation of *ortho*-methyl groups on the meso-aryl rings is shown in Figure 1, which displays the conformation of the meso-aryl ring relative to the porphyrin macrocycle. The meso-aryl ring lacking any *ortho*-methyl groups can rotate toward coplanarity with the porphyrin macrocycle, thereby increasing π-conjugation and enhancing the interporphyrin electronic communication that underpins hole/electron transfer.[24] In contrast, the meso-aryl ring that bears two *ortho*-methyl groups is torsionally constrained toward such rotation, whereupon the electronic communication is

dx.doi.org/10.1021/ic301613k | *Inorg. Chem.* XXXX, XXX, XXX−XXX

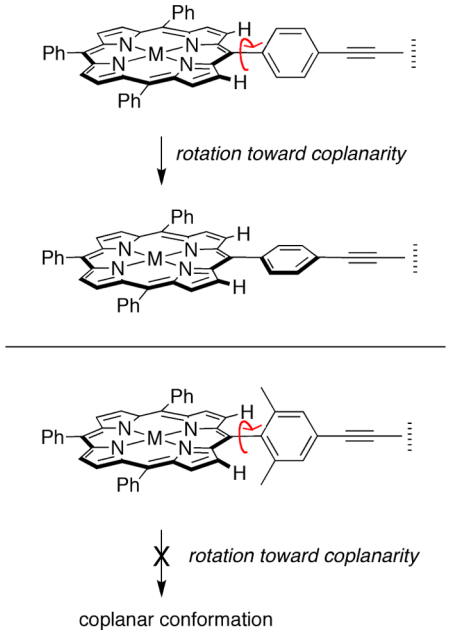

Figure 1. Absence or presence of torsional constraints on meso-aryl rotation.

expected to diminish. Accordingly, studies of the dyads shown in Chart 1 unambiguously elucidate the origin of the activation process for hole/electron transfer in the porphyrin dyads.

II. RESULTS

A. Synthesis. A set of *meso*-substituted porphyrins was prepared wherein each porphyrin bears phenyl groups at the 5,10,15-positions and an ethynylaryl or iodoaryl group at the 20-position. The ethynylaryl or iodoaryl groups are unsubstituted at the 2,6-positions or bear 2,6-dimethyl groups to inhibit rotation of the aryl group toward coplanarity with the porphyrins.[24] Each of the porphyrins bearing an iodo group (**Fb-H-I**,[24] **Fb-U-I**[25,26]) or trimethylsilylethynyl group (**Fb-H-TMS**,[24] **Fb-U-TMS**[27]) has been prepared previously using statistical techniques. Here, the same porphyrins were prepared in a rational manner by coupling dipyrromethane-dicarbinol (**1-OH**) and a dipyrromethane (**2a**–**d**) respectively, using a literature procedure.[28] The procedure entailed reaction in CH_2Cl_2 containing $Sc(OTf)_3$ (2.8 mM) and 2,6-di-*tert*-butylpyridine (2,6-DTBP) (28 mM) at room temperature followed by oxidation with DDQ. The putative dipyrromethane-dicarbinol (**1-OH**) was obtained by the reduction of diacyldipyrromethane–tin complex **1** using $NaBH_4$ (Scheme 1).[28–30]

Treatment of the trimethylsilylethynylporphyrins **Fb-H-TMS** and **Fb-U-TMS** to fluoride-mediated deprotection (using tetrabutylammonium fluoride) in THF unveiled the ethyne moiety and afforded porphyrins **Fb-H** and **Fb-U**, respectively. The latter porphyrin also has been prepared previously,[27,31] whereas the former has been employed as the zinc chelate.[24] The thallium(III) complexes of porphyrins **Fb-H** and **Fb-U** were prepared by treating the free base with excess $TlCl_3{\cdot}4H_2O$ (Scheme 2).

The *meso*-substituted diphenylethyne-linked porphyrin dyads were obtained by the copper-free, palladium mediated Sonogashira coupling of an iodophenylporphyrin and an ethynylphenylporphyrin.[32,33] The reaction of **Fb-H** and **Fb-H-I**, **Fb-U** and **Fb-H-I**, and **Fb-U** and **Fb-U-I** with $Pd_2(dba)_3$ and $P(o\text{-tol})_3$ in toluene/triethylamine (5:1) at 40 °C for 6 h afforded $\mathbf{Fb_2}$**-B**, $\mathbf{Fb_2}$**-M**, and $\mathbf{Fb_2}$**-U** in 47%, 41%, and 28% yield, respectively. Treatment of the three free base dyads with excess $TlCl_3{\cdot}4H_2O$ in CH_2Cl_2/CH_3OH at room temperature[34] for 6 h provided the corresponding thallium dyads in 51–62% yield (Scheme 3).

Scheme 1. Rational Synthesis of Free Base Porphyrin Building Blocks

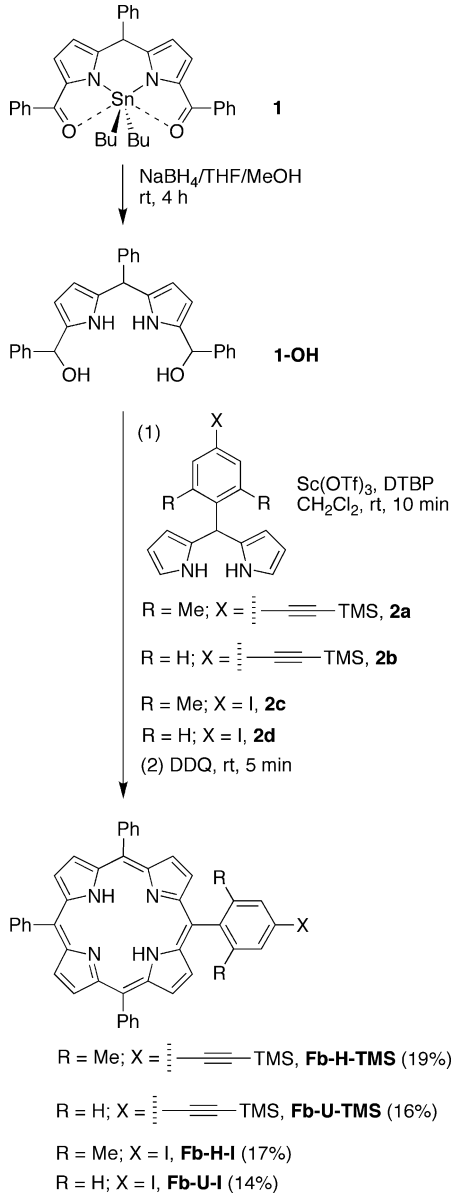

B. EPR Spectra of the Monocations of the Thallium-Chelated Monomers. The room-temperature EPR spectra of the monocations of **Tl-U** and **Tl-H** are shown in Figure 2. The EPR spectra of the thallium-chelated porphyrins exhibit a simple hyperfine doublet arising from coupling of the unpaired electron spin with the I = 1/2 thallium nuclei. The $^{203}Tl/^{205}Tl$ hyperfine coupling for the monocations of **Tl-U** and **Tl-H** are 11.1 and 16.8 G, respectively. No additional hyperfine structure is observed; such structure might have arisen due to resolving of the hyperfine doublets of the ^{203}Tl and ^{205}Tl nuclei or resolving of the nine-line pattern expected from the ^{14}N nuclei. These characteristics of the EPR spectra of the monocations of

dx.doi.org/10.1021/ic301613k | Inorg. Chem. XXXX, XXX, XXX–XXX

Scheme 2. Synthesis of Thallium(III)-Containing Porphyrin Building Blocks

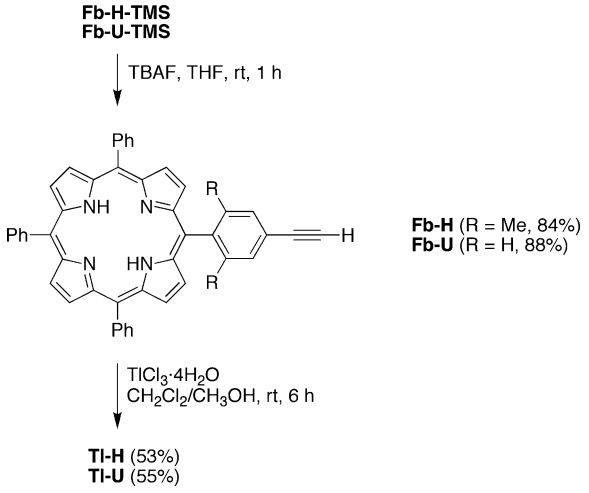

Scheme 3. Directed Synthesis of Diarylethyne-Linked Thallium(III) Porphyrin Dyads

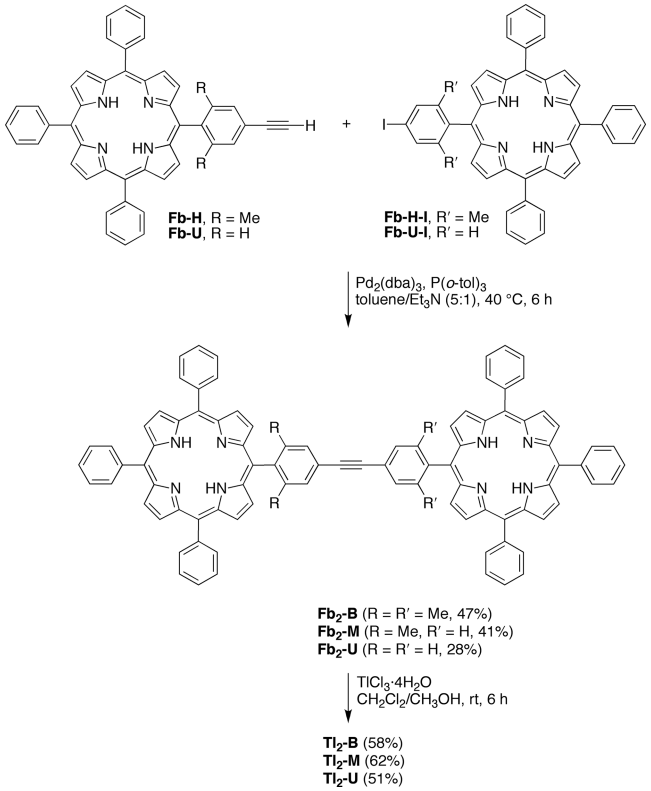

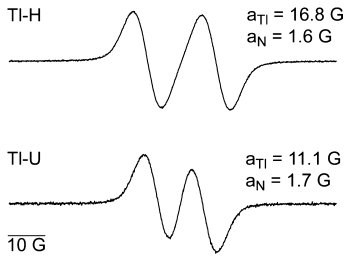

Figure 2. Room-temperature EPR spectra of the monocations of **Tl-U** and **Tl-H**.

the thallium-chelated monomers are similar to those we have previously observed for the thallium chelates of other types of porphyrins.[23] [Note that the ^{14}N hyperfine couplings reported in Figure 2 and elsewhere herein are obtained from simulations that indicate that inclusion of this coupling gives a better fit to the line shape.]

The observation that the presence of an *ortho*-dimethylaryl group affects the magnitude of ^{203}Tl/^{205}Tl hyperfine couplings (**Tl−U**, 11.1G; **Tl−H**, 16.8 G) is further consistent with our previous studies on thallium-chelated porphyrins that contain three mesityl groups at the non-linking meso positions of the porphyrin ring and an aryl ring that lacks any *ortho*-methyl substituents at the linker position.[23] The ^{203}Tl/^{205}Tl hyperfine couplings for the monocation of this latter porphyrin (24.9 G), which contains three meso groups with *ortho*-dimethylaryl substitution, are larger than those for either **Tl−U** (11.1 G) or **Tl−H** (16.8 G), which contain zero or one group with *ortho*-dimethylaryl substitution, respectively. The ^{203}Tl/^{205}Tl hyperfine couplings in the monocation of thallium-chelated tetramesitylporphyrin, which contains four meso groups with *ortho*-dimethylaryl substitution, are larger still (27 G) and further consistent with the trend (unpublished results).

One possible explanation for the increase in ^{203}Tl/^{205}Tl hyperfine couplings as the number of meso *ortho*-dimethylaryl substituents increases is that steric interactions between the methyl groups and the thallium ion force the metal more in-plane thereby enhancing the degree of metal−porphyrin orbital mixing. However, this view is not consistent with the results of density functional theory (DFT) calculations on the various porphyrins that predict that the extent of doming of the porphyrin is not affected by the addition of *ortho*-dimethylaryl substituenst. Accordingly, the change in the magnitude of the ^{203}Tl/^{205}Tl hyperfine couplings as the number of meso *ortho*-dimethylaryl substituents increases must arise from subtle electronic effects. These electronic effects must indeed be small because the potentials of the first oxidation of **Tl-U** and **Tl-H** are the same to within experimental error (< ± 0.02 V). Likewise the energies of the HOMOs of the two porphyrins are essentially identical (vide infra).

C. EPR Spectra of the Monocations of the Tl_2-U, Tl_2-M, and Tl_2-B Dyads. The variable-temperature EPR spectra of the monocations of **Tl_2-U**, **Tl_2-M**, and **Tl_2-B** are shown in the left panels of Figures 3, 4, and 5, respectively. For all three dyads, spectra are not shown at temperatures below the 160−170 K range because the solvent/electrolyte mixture freezes and the spectra change abruptly and become extremely broad. Spectra were not obtained above the 320−340 K range owing to solvent volatility.

The EPR spectra of the monocations of **Tl_2-U** (Figure 3) and **Tl_2-M** (Figure 4) are qualitatively similar to one another. The spectra both exhibit a three-line ^{203}Tl/^{205}Tl hyperfine pattern at room temperature, which gradually evolves into a two-line hyperfine pattern as the temperature is lowered. The EPR spectra of the monocation of **Tl_2-B** (Figure 5) are somewhat different in that the three-line pattern ^{203}Tl/^{205}Tl hyperfine pattern is much less pronounced at higher temperatures.

Simulations of the variable-temperature EPR spectra of the monocations of **Tl_2-U**, **Tl_2-M**, and **Tl_2-B** are shown on the right sides of Figures 3, 4, and 5, respectively. The ^{203}Tl/^{205}Tl and ^{14}N hyperfine couplings and line widths used for all the simulations are compiled in Table S1 (Supporting Information). The hole/electron-transfer rate constants derived from the simulations are shown above each spectral trace. At room

dx.doi.org/10.1021/ic301613k | Inorg. Chem. XXXX, XXX, XXX−XXX

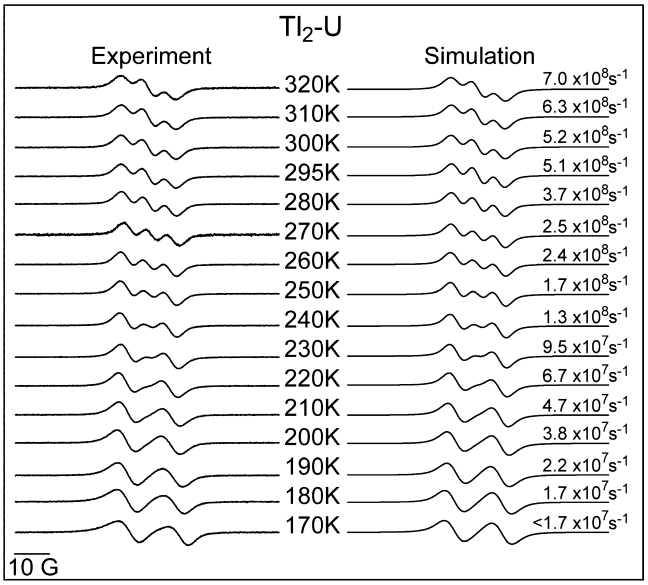

Figure 3. Variable-temperature EPR spectra of the monocation of **Tl_2-U** (left) and simulated spectra (right) with derived hole-transfer rates.

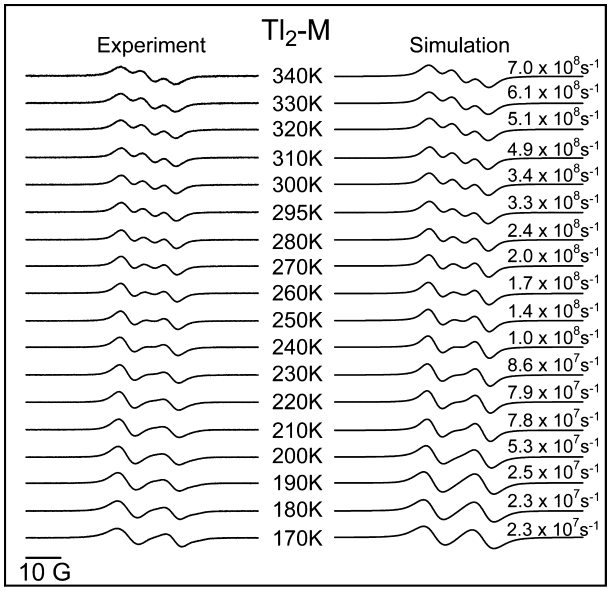

Figure 4. Variable-temperature EPR spectra of the monocation of **Tl_2-M** (left) and simulated spectra (right) with derived hole-transfer rates.

temperature (295 K), the hole/electron-transfer rate constants for **Tl_2-U**, **Tl_2-M**, and **Tl_2-B** are 5.1×10^8 s^{-1}, 3.3×10^8 s^{-1}, and 1.6×10^8 s^{-1}, respectively. The simulations further indicate that the decrease in rate as the temperature is lowered becomes less pronounced as *ortho*-dimethyl groups are added to the aryl group of the linker. Indeed, for the monocation of **Tl_2-B**, the hole/electron-transfer rate does not change appreciably over the 160−340 K temperature range.

To probe further the temperature dependence of hole/electron-transfer, the rate constants were plotted logarithmically versus $1/T$. Plots of $kT^{1/2}$ versus $1/T$ for the monocations of **Tl_2-U**, **Tl_2-M**, and **Tl_2-B** are shown in Figure 6. This approach assumes hole/electron transfer can be modeled using the semiclassical Marcus equation in the nonadiabatic limit,[35]

$$k = AT^{-1/2}\exp(-\Delta G^{\ddagger}/k_B T) \quad (1)$$

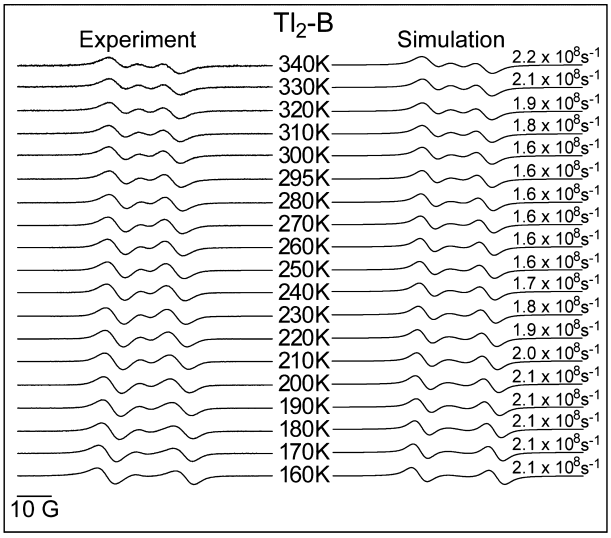

Figure 5. Variable-temperature EPR spectra of the monocation of **Tl_2-B** (left) and simulated spectra (right) with derived hole-transfer rates.

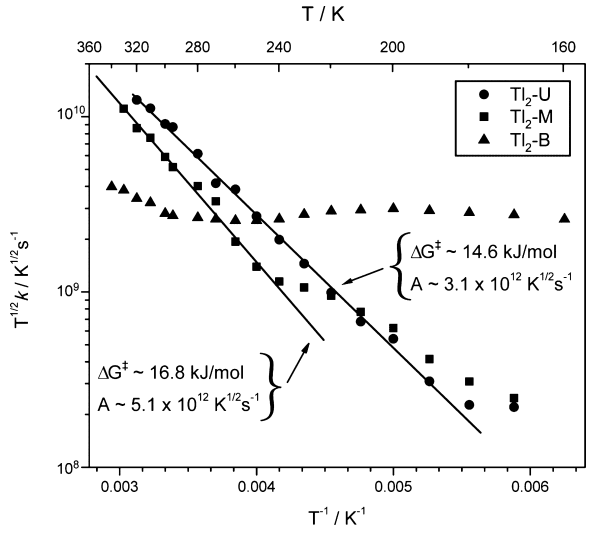

Figure 6. Marcus-equation plots for the monocations of **Tl_2-U**, **Tl_2-M**, and **Tl_2-B**.

where $\Delta G^{\ddagger} = (\Delta G_o + \lambda)^2/4\lambda$; $A = (4\pi^3/h^2\lambda k_B)^{1/2}|V^2|$; ΔG_o is the free energy change associated with hole/electron transfer; λ is the reorganization energy; and V is the effective electronic coupling. Both **Tl_2-U** and **Tl_2-B** are symmetrical; thus, the electron-donor and -acceptor thallium porphyrins are redox equivalent (isoenergetic) and the hole/electron-transfer process has $\Delta G_o = 0$. **Tl_2-M** is not rigorously symmetrical; however, as noted above, the redox potentials of the constituent porphyrins are the same to within experimental error. Likewise, the difference in the energies of HOMOs of the constituent porphyrins is minimal (vide infra). Thus, the hole/electron transfer in the monocation of this dyad is also taken to have $\Delta G_o = 0$.

Inspection of Figure 6 reveals the following key features.

(1) The plot for the monocation of **Tl_2-U** exhibits a positive slope over the 170−320 K temperature range. The data are well fit with eq 1; however, nearly equivalent fits are obtained using eq 1 in the adiabatic limit (no T dependence in the prefactor). The values of $\Delta G^{\ddagger} \sim 14.6$ kJ/mol and $A \sim 3.1 \times 10^{12}$ K s^{-1} are

dx.doi.org/10.1021/ic301613k | Inorg. Chem. XXXX, XXX, XXX−XXX

obtained from the slope and intercept of the linear fits to the data using eq 1.

(2) The plot for the monocation of **Tl_2-M** differs somewhat from that of **Tl_2-U** in that only the region above 240 K is well fit via eq 1 (or the adiabatic equivalent) and yields $\Delta G^{\ddagger} \sim 16.8$ kJ mol^{-1} and A $\sim 5.1 \times 10^{12}$ K s^{-1}. Below 240 K, the data are somewhat irregular, exhibiting a generally less positive slope than the data above 240 K.

(3) The plot for the monocation of **Tl_2-B** is essentially flat over the 160−340 K temperature range, albeit there appears to be an onset of a slight positive slope above 300 K. Regardless, the data are indicative of an essentially activationless hole/electron-transfer process ($\Delta G^{\ddagger} < k_B T$).

D. Molecular Orbital Characteristics of the Thallium Porphyrins and Linkers. To gain insight into the relative energies of the molecular orbitals of the porphyrins and linkers in the dyads, DFT calculations were performed on a series of model compounds. The focus of these calculations was the relative energies of the HOMOs of the molecules, which are the key orbitals for the hole/electron-transfer process. The two porphyrin model compounds included a thallium chelate with four meso-phenyl substituents and a thallium chelate with three meso-phenyl and one meso-mesityl substituents. The three linker model compounds included 1,2-di-*p*-tolylethyne (**U**), 1,2-bis(3,4,5-trimethylphenyl)ethyne (**B**), and an ethynyl species containing one *p*-tolyl and one 3,4,5-trimethylphenyl group (**M**). The terminal methyl group (para position in tolyl, 4-position in 3,4,5-trimethylphenyl) is included to represent the 20-carbon of the porphyrin to which the linker would be attached; thus, the *p*-tolyl group models the unsubstituted aryl unit whereas the 3,4,5-trimethylphenyl group models the aryl unit bearing two *o*-methyl groups.

The calculated electron densities and energies for the HOMOs and lowest unoccupied molecular orbitals (LUMOs) of the two porphyrins and three linkers are shown in Figure 7. The structures of the molecules are included in the figure. The calculations predict that the HOMO energies for the two porphyrins are essentially identical (−5.25 eV). This result supports the approximation that $\Delta G_o \sim 0$ for the hole/electron-transfer process in the monocation of **Tl_2-M**. The calculations for the **U**, **M**, and **B** linkers further predict that the HOMO energies change relatively modestly as *ortho*-dimethyl groups are added to the basic diarylethyne structure (−5.46 eV versus −5.36 eV versus −5.27 eV).

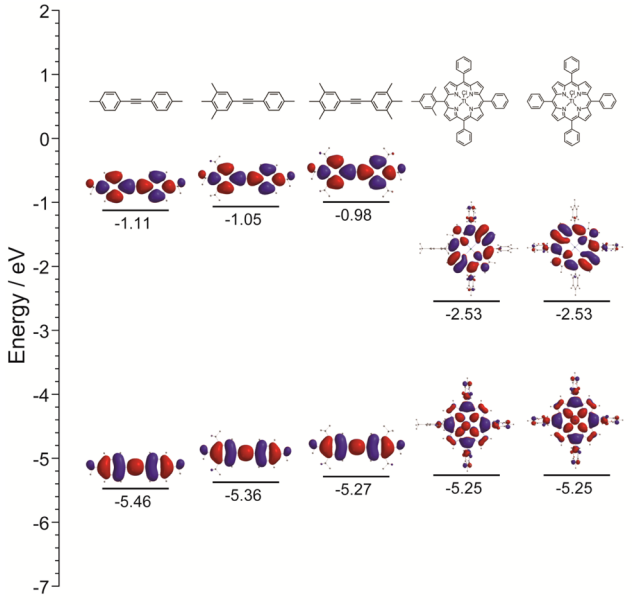

Figure 7. Calculated electron densities and energies for the HOMOs and LUMOs of the **U**, **M**, and **B** linkers and of two model thallium porphyrins.

III. DISCUSSION

We have examined the hole/electron-transfer process in a series of singly oxidized thallium-chelated porphyrin dyads wherein the torsional constraints in the linker are systematically increased (**Tl_2-U** < **Tl_2-M** < **Tl_2-B**). Many of the general characteristics of the hole/electron-transfer process in the monocations of these dyads are similar to those we have previously reported for other types of thallium-chelated porphyrin dyads.[23] We will not focus on these characteristics herein. Instead, the reader is referred to our previous work for detailed discussion.

The key observations from the present studies are as follows: (1) Hole/electron-transfer at room temperature (295 K) in the monocations of **Tl_2-U**, **Tl_2-M**, and **Tl_2-B** occurs at rates that correspond to time scales in the 2−5 ns regime. (2) Hole/electron transfer at room temperature (295 K) slows as torsional constraints are added to the basic diarylethyne linker [k(**Tl_2-U**) > k(**Tl_2-M**) > k(**Tl_2-B**)]. (3) As the temperature decreases, the hole/electron-transfer rates for the monocations of the three types of dyads converge and then cross over. At the lowest temperatures examined (160−170 K), the trend in the hole/electron-transfer rates is essentially reversed [k(**Tl_2-B**) > k(**Tl_2-M**) ∼ k(**Tl_2-U**)].

The trends in the hole/electron-transfer rates exhibited by the monocations of **Tl_2-U**, **Tl_2-M**, and **Tl_2-B** as a function of temperature arise because the thermal-activation behavior of the process is different among the three types of dyads. In the case of the monocation of **Tl_2-U**, hole/electron transfer is (weakly) thermally activated over the full temperature range examined, whereas for the monocation of **Tl_2-B**, hole/electron transfer is essentially activationless over this temperature range. In the case of the monocation of **Tl_2-M**, hole/electron transfer is (weakly) activated at room temperature (and somewhat below), but appears to trend toward a less-activated (activationless) regime at lower temperature. In this respect, the thermal-activation behavior exhibited by the monocation of **Tl_2-M** is intermediate between that exhibited by the monocations of **Tl_2-U** and **Tl_2-B**.

We have previously proposed that the most self-consistent explanation for the activation behavior observed for the hole/electron-transfer process in the monocations of the porphyrin dyads is that torsional motions of the aryl rings in the linker contribute to the process. In this picture, rotation of the aryl rings toward coplanarity with the porphyrin would enhance hole/electron transfer via an increase in a conjugative pathway between the two porphyrins. The results of the present study are consistent with this view. The addition of *ortho*-dimethyl groups to the basic diarylethyne linker, which substantially increases the torsional barrier for ring rotation,[36] appears to systematically diminish the thermal activation of hole/electron-transfer. Indeed, in the case of the monocation of **Tl_2-B**, in which both aryl rings of the linker are highly constrained from tending toward coplanarity with the porphyrin ring, the hole/electron-transfer process is essentially activationless.

dx.doi.org/10.1021/ic301613k | *Inorg. Chem.* XXXX, XXX, XXX−XXX

As we have previously discussed,[23] the $\Delta G^{\ddagger}$ values determined for all the porphyrin dyads are much smaller than the measured aryl-ring torsional barriers in meso-substituted porphyrins. These barriers are in the 60−100 kJ mol^{-1} range.[36] Thus, any type of torsional motion that might contribute to activation of the hole/electron-transfer process in the monocations of the porphyrin dyads would necessarily involve only restricted rotation of the aryl ring toward coplanarity with the porphyrin. In particular, the faster rates at higher temperature are due to an increase in the amplitude of the low-frequency, large-amplitude torsional motions that occurs upon population of higher vibrational states in the torsional potential energy well.

One characteristic of the thermal behavior of the hole/electron-transfer process in the monocations of **Tl_2-U**, **Tl_2-M**, and **Tl_2-B** that is puzzling is the reversal in the rates along the series of dyads as the temperature is lowered. One plausible explanation is that electronic rather than torsional effects dominate at lower temperatures. This view is qualitatively consistent with the relative energies of the HOMOs of the **U**, **M**, and **B** linkers relative to those of the thallium-chelated porphyrins (Figure 7). As *ortho*-dimethyl groups are added to the linker, the energy of the linker HOMO becomes less negative and approaches (but remains lower than) that of the thallium-chelated porphyrins. The most consistent explanation is if the linker HOMOs remain sufficiently below those of the porphyrins so that hole/electron transfer proceeds by a superexchange mechanism (tunneling rather than hopping). Within that mechanism, as we have previously discussed, the difference in energies (ΔE_{PL}) of the HOMOs of the linker and porphyrin are related to the height of the tunneling barrier for hole/electron transfer—the smaller the ΔE_{PL} the lower the tunneling barrier.[23] The prediction that the value of ΔE_{PL} becomes smaller along the series [ΔE_{PL}(**Tl_2-U**) > ΔE_{PL}(**Tl_2-M**) > ΔE_{PL}(**Tl_2-B**)] would be consistent with the monocation of **Tl_2-B** exhibiting the fastest rate at lower temperature. This picture is basically a static view of the hole/electron-transfer process. As the temperature increases, torsional dynamics come into play and then dominate the hole/electron-transfer process at more elevated temperatures.

Finally, we note that the temperature dependence observed in our previous study of hole/electron transfer in the monocations of a series of (*p*-phenylene)$_n$-linked dyads parallels that observed for the monocations of **Tl_2-U**, **Tl_2-M**, and **Tl_2-B**. The rates for the (*p*-phenylene)$_n$-linked dyads at room temperature monotonically decrease as the number of *p*-pheneylene units in the linker increases from one to four. As the temperature is lowered, the rates cross over, and at low temperature, the trend is reversed. However, the calculated ΔE_{PL} values for the *p*-phenylene linkers also monotonically decrease as the number of *p*-phenylene units in the linker increases. Consequently, the barrier to hole/electron-transfer would become lower. Collectively, this interplay of electronic and torsional effects might then also explain the temperature dependence of the activation behavior of hole/electron transfer in the monocations of the (*p*-phenylene)$_n$-linked dyads.

IV. OUTLOOK

The rational design of molecular architectures that support artificial photosynthesis and molecular electronics requires a deep understanding of the factors that affect electronic interactions between constituent chromophores. Ground-state hole/electron transfer is central to many solar energy-transduction processes and to information storage in molecular electronics. In the architectures studied herein, the diarylethyne linker provides a conduit for ground-state hole/electron transfer between two porphyrins. Pinpointing the rates of hole/electron transfer has heretofore proved somewhat difficult. Application of the recently demonstrated ^{203}Tl/^{205}Tl hyperfine "clocking" strategy to a series of three diarylethyne-linked porphyrin dyads enabled determination of the rates of ground-state hole/electron transfer, and, in conjunction with variable temperature studies, delineated the effects of torsional constraints on such rates.

The finding that ground-state hole/electron transfer at room temperature (295 K) slows as torsional constraints are added to the diarylethyne linker [k(**Tl_2-U**) > k(**Tl_2-M**) > k(**Tl_2-B**)] is not surprising, but knowledge of the exact rate constants (k ranges from 5.1 × 10^8 s^{-1} to 1.6 × 10^8 s^{-1} at 295 K) was heretofore not known. The change in rate constant by a factor of ∼3.2 is consistent with results for excited-state energy transfer, excited-state hole−electron transfer, and ground-state hole/electron transfer in the same molecular architectures wherein one porphyrin is a zinc chelate and the other is a free base.[13,18,37a,b] The excited-state energy transfer process also is dominated by a through-bond mechanism mediated by the diarylethyne linker. The general time scale and diminution in rate constant found here for ground-state hole/electron transfer between thallium porphyrins are consistent with the values obtained at 295 K using transient absorption spectroscopy for zinc porphyrins with no steric constraints (k = 12.5 × 10^8 s^{-1}) or steric hindrance on one aryl ring of the linker (k = 8.3 × 10^8 s^{-1}).[37c] Variable-temperature studies here have revealed the subtle interplay of steric factors (torsional constraints on the linker) and electronic factors for ground-state hole/electron transfer; thus, the energy of activation for hole/electron transfer ($\Delta G^{\ddagger}$) is ∼14.6 kJ/mol for **Tl_2-U**, ∼ 16.8 kJ mol^{-1} for **Tl_2-M**, and < k_BT (i.e., essentially activationless) for **Tl_2-B**. Such data should be of value in the rational design of multicomponent molecular architectures that convey holes/electrons in diverse schemes for artificial photosynthesis and molecular electronics.

V. EXPERIMENTAL SECTION

A. General Methods. ^{1}H NMR spectra (300 MHz) were collected at room temperature in $CDCl_3$ unless noted otherwise. Silica gel (40 μm average particle size) was used for column chromatography. Matrix assisted laser desorption ionization mass spectrometry (MALDI-MS) employed a matrix of 1,4-bis(5-phenyl-2-oxazol-2-yl)benzene.[38] Electrospray ionization mass spectrometry (ESI-MS) data are reported for the molecular ion or protonated molecular ion. The palladium-coupling reactions were carried out using Schlenk-line techniques. Size-exclusion chromatography (SEC) was performed as described previously.[39]

B. Solvents. All solvents were reagent grade and were used as received unless noted otherwise. THF was freshly distilled from sodium/benzophenone ketyl.

C. Noncommercial Compounds. Dipyrromethanes **1**,[29] **2a**,[40,41] **2b**,[41] **2c**,[40,41] and **2d**[42] were prepared as described in the literature.

D. Electrochemistry. The electrochemical measurements were performed using techniques and instrumentation previously described.[43] The sample concentrations were at levels that preclude intermolecular disproportionation reactions which would result in formation of dication radical species.[17,18] The samples were contained in a three-compartment cell equipped with a Pt wire working electrode, a Pt mesh counter electrode, and a Ag/Ag$^+$ (butyronitrile) reference electrode. The solvent was CH_2Cl_2 containing 0.1 M Bu_4NPF_6 as the supporting electrolyte. All reported potentials are with respect to ferrocene/ferrocenium = 0.19 V. The bulk-oxidized

dx.doi.org/10.1021/ic301613k | Inorg. Chem. XXXX, XXX, XXX−XXX

complexes were prepared in a glovebox via quantitative coulometric bulk electrolysis at a Pt mesh electrode. The integrity of the samples was checked by cyclic voltammetry after each successive oxidation. Upon oxidation, the samples were transferred to an EPR tube and sealed in the glovebox.

E. EPR Spectroscopy and Simulations. The EPR spectra were recorded on an X-band spectrometer (Bruker EMX) equipped with an NMR gaussmeter and microwave frequency counter. The EPR spectra were obtained on samples that were typically 0.2 mM. The microwave power and magnetic field modulation amplitude were typically 5.7 mW and 0.32 G, respectively.

The EPR spectra of the monocations of the monomers were simulated with the WinSim program to obtain the values of the $^{203/205}$Tl and ^{14}N hyperfine coupling constants and linewidths.[44] The EPR spectra of the monocations of the dyads were simulated with the ESR-EXN program.[45,46] This program and its application to extract exchange rates from isotropic EPR spectra have been described in detail elsewhere.[45] The hyperfine coupling constants and line widths obtained from the simulations of the spectra of the monocations of the monomers were used as the initial values of these parameters in the simulations of the spectra of the monocations of the dyads. Prior to initiating the latter simulations, it was confirmed that the EPR spectra of the monocations of the monomers were faithfully reproduced by the ESR-EXN program using the parameters obtained from the WinSim program. The hole/electron-transfer rates at the different temperatures were derived from the simulations of the variable-temperature EPR spectra of the monocations of the dyads. The rate constants were adjusted manually to provide a best fit to the spectra as judged by the residuals between the observed and simulated spectra. Changes in the rate constants of ±10% from the best fit values resulted in clearly poorer fits to the spectra. Finally, the hyperfine coupling constants and line widths vary somewhat with temperature (a few percent); consequently, these parameters were adjusted to optimize the fits of the EPR spectra obtained at the different temperatures.

F. Molecular Orbital Calculations. DFT calculations were performed with Spartan '08 for Windows 1.2.0[47] in parallel mode on a PC equipped with an Intel i7-975 CPU, 24 GB ram, and three 300-GB, 10k-rpm hard drives. The hybrid B3LYP functional and the LACVP basis set were employed. The equilibrium geometries were fully optimized using the default parameters of the Spartan '08 program.

G. Synthesis Procedures. *5,10,15-Triphenyl-20-[2,6-dimethyl-4-[2-(trimethylsilyl)ethynyl]phenyl]porphyrin (**Fb-H-TMS**).* Following a reported procedure,[28] the condensation of dicarbinol **1-OH** [derived from reduction of **1** (1.09 g, 1.65 mmol) with $NaBH_4$ (1.24 g, 33.0 mmol) in THF/MeOH (132 mL, 3:1)] and dipyrromethane **2a** (571 mg, 1.65 mmol) was carried out in the presence of 2,6-di-*tert*-butylpyridine (481 μL, 2.14 mmol) and $Sc(OTf)_3$ (105 mg, 0.214 mmol) in CH_2Cl_2 (76 mL) at room temperature for 10 min followed by the addition of DDQ (1.12 g, 4.95 mmol). After 5 min, the reaction mixture was filtered through a pad of alumina (CH_2Cl_2 containing 0.1% triethylamine). The resulting porphyrin-containing solution was concentrated to give a purple solid. Methanol was added. The resulting suspension was sonicated for 5 min and then filtered through filter paper. The filtered material was washed with methanol and dried in vacuo to afford a crystalline purple solid (231 mg, 19%): ^{1}H NMR, mass, and UV−vis spectral data were consistent with our data for the preparation via an alternative route.[24]

*5,10,15-Triphenyl-20-[4-[2-(trimethylsilyl)ethynyl]phenyl]-porphyrin (**Fb-U-TMS**).* Following a reported procedure,[28] the condensation of dicarbinol **1-OH** [derived from reduction of **1** (1.43 g, 2.16 mmol) with $NaBH_4$ (4.08 g, 108 mmol) in THF/MeOH (175 mL, 3:1)] and dipyrromethane **2b** (688 mg, 2.16 mmol) was carried out in the presence of 2,6-di-*tert*-butylpyridine (628 μL, 2.80 mmol) and $Sc(OTf)_3$ (138 mg, 0.280 mmol) in CH_2Cl_2 (100 mL) at room temperature for 10 min followed by the addition of DDQ (1.47 g, 6.48 mmol). After 5 min, the reaction mixture was filtered through a pad of alumina (CH_2Cl_2 containing 0.1% triethylamine). The resulting porphyrin-containing solution was concentrated to give a purple solid. Methanol was added. The resulting suspension was sonicated for 5 min and then filtered through filter paper. The filtered material was washed with methanol and dried in vacuo to afford a crystalline purple solid (245 mg, 16%): ^{1}H NMR (300 MHz, $CDCl_3$) δ −2.78 (br, 2H), 0.37 (s, 9H), 7.68−7.80 (m, 9H), 7.86 (d, J = 8.1 Hz, 2H), 8.16 (d, J = 8.1 Hz, 2H), 8.18−8.24 (m, 6H), 8.78−8.88 (m, 8H); MALDI-MS obsd 711.0; ESI-MS obsd 711.2938, calcd 711.2939 [(M + H)$^+$, M = $C_{49}H_{38}N_4Si$]; λ_{abs} (CH_2Cl_2) 418, 515, 551, 589 nm. The data are in close agreement with those for the preparation via an alternative route.[27]

*5,10,15-Triphenyl-20-[2,6-dimethyl-4-ethynylphenyl]porphyrin (**Fb-H**).* A solution of porphyrin **Fb-H-TMS** (147 mg, 200 μmol) in THF (20 mL) was treated with 1 M TBAF in THF (300 μL, 300 μmol). The reaction mixture was stirred at room temperature for 1 h under argon. The reaction mixture was concentrated to dryness. The resulting purple solid was dissolved in CH_2Cl_2 (50 mL). The organic solution was washed with saturated aqueous $NaHCO_3$ and water, dried (Na_2SO_4), and concentrated. Column chromatography [silica, CH_2Cl_2/hexanes (1:1)] provided a purple solid (112 mg, 84%): ^{1}H NMR (300 MHz, $CDCl_3$) δ −2.70 (br, 2H), 1.86 (s, 6H), 3.24 (s, 1H), 7.63 (s, 2H), 7.68−7.82 (m, 9H), 8.18−8.26 (m, 6H), 8.65 (d, J = 4.8 Hz, 2H), 8.82 (d, J = 4.8 Hz, 2H), 8.83 (s, 4H); MALDI-MS obsd 666.5; ESI-MS obsd 667.2847, calcd 667.2856 [(M + H)$^+$, M = $C_{48}H_{34}N_4$]; λ_{abs} (CH_2Cl_2) 418, 485, 513, 548, 592 nm.

*5,10,15-Triphenyl-20-(4-ethynylphenyl)porphyrin (**Fb-U**).* A solution of porphyrin **Fb-U-TMS** (142 mg, 200 μmol) in THF (20 mL) was treated with 1 M TBAF in THF (300 μL, 300 μmol). The reaction mixture was stirred at room temperature for 1 h under argon. The reaction mixture was concentrated to dryness. The resulting purple solid was dissolved in CH_2Cl_2 (50 mL). The organic solution was washed with saturated aqueous $NaHCO_3$ and water, dried (Na_2SO_4) and concentrated. Column chromatography [silica, CH_2Cl_2/hexanes (1:1)] provided a purple solid (112 mg, 88%): ^{1}H NMR (300 MHz, $CDCl_3$) δ −2.79 (br, 2H), 3.31 (s, 1H), 7.70−7.80 (m, 9H), 7.89 (d, J = 8.4 Hz, 2H), 8.16−8.24 (m, 8H), 8.78−8.88 (m, 8H); MALDI-MS obsd 638.3; ESI-MS obsd 639.2541, calcd 639.2543 [(M + H)$^+$, M = $C_{46}H_{30}N_4$]; λ_{abs} (CH_2Cl_2) 418, 515, 550, 591 nm. The data are in close agreement with those for the preparation via an alternative route.[27,31]

*5,10,15-Triphenyl-20-(2,6-dimethyl-4-iodophenyl)porphyrin (**Fb-H-I**).* Following a reported procedure,[28] the condensation of dicarbinol **1-OH** [derived from reduction of **1** (952 mg, 1.44 mmol) with $NaBH_4$ (2.72 g, 72.0 mmol) in THF/MeOH (115 mL, 3:1] and dipyrromethane **2c** (541 mg, 1.44 mmol) was carried out in the presence of 2,6-di-*tert*-butylpyridine (420 μL, 1.87 mmol) and $Sc(OTf)_3$ (92.0 mg, 0.187 mmol) in CH_2Cl_2 (67 mL) at room temperature for 10 min followed by the addition of DDQ (980 mg, 4.32 mmol). After 5 min, the reaction mixture was filtered through a pad of alumina (CH_2Cl_2 containing 0.1% triethylamine). The resulting porphyrin-containing solution was concentrated to give a purple solid. Methanol was added. The resulting suspension was sonicated for 5 min and then filtered through filter paper. The filtered material was washed with methanol and dried in vacuo to afford a crystalline purple solid (188 mg, 17%): ^{1}H NMR, mass, and UV−vis spectral data were consistent with our data for the preparation via an alternative route.[24]

*5,10,15-Triphenyl-20-(4-iodophenyl)porphyrin (**Fb-U-I**).* Following a reported procedure,[28] the condensation of dicarbinol **1-OH** [derived from reduction of **1** (569 mg, 860 μmol) with $NaBH_4$ (1.62 g, 43.0 mmol) in THF/MeOH (69 mL, 3:1)] and dipyrromethane **2d** (300 mg, 860 μmol) was carried out in the presence of 2,6-di-*tert*-butylpyridine (251 μL, 1.12 mmol) and $Sc(OTf)_3$ (55.0 mg, 0.112 mmol) in CH_2Cl_2 (40 mL) at room temperature for 10 min followed by the addition of DDQ (586 mg, 2.58 mmol). After 5 min, the reaction mixture was filtered through a pad of alumina (CH_2Cl_2 containing 0.1% triethylamine). The resulting porphyrin-containing solution was concentrated to give a purple solid. Methanol was added. The resulting suspension was sonicated for 5 min and then filtered through filter paper. The filtered material was washed with methanol and dried in vacuo to afford a crystalline purple solid (92 mg, 14%): ^{1}H NMR (300 MHz, $CDCl_3$) δ −2.80 (br, 2H), 7.68−7.82 (m, 9H), 7.94 (d, J = 8.1 Hz, 2H), 8.08 (d, J = 8.1 Hz, 2H), 8.18−8.26 (m, 6H), 8.78−8.90 (m, 8H); MALDI-MS obsd 741.1; ESI-MS obsd 741.1503,

dx.doi.org/10.1021/ic301613k | Inorg. Chem. XXXX, XXX, XXX−XXX

calcd 741.1510 [$(M + H)^+$, M = $C_{44}H_{29}IN_4$]; λ_{abs} (CH_2Cl_2) 418, 514, 549, 590 nm. The data are in close agreement with those for the preparation via an alternative route.[25,26]

*1,2-Bis[4-(5,10,15-triphenylporphin-20-yl)-3,5-dimethylphenyl]-ethyne (**Fb$_2$-B**).* Following a copper-free procedure for Sonogashira coupling of porphyrins,[32,33] samples of **Fb-H** (35.5 mg, 53.2 μmol), **Fb-H-I** (40.8 mg, 53.2 μmol), and P(*o*-tol)$_3$ (19.4 mg, 63.8 μmol) in toluene/triethylamine [(5:1), 21 mL) were degassed by three freeze/pump/thaw cycles. Then $Pd_2(dba)_3$ (7.3 mg, 8.0 μmol) was added, and the mixture was additionally degassed by three freeze/pump/thaw cycles. The resulting mixture was stirred for 6 h at 40 °C in a Schlenk line. The reaction mixture was allowed to cool and then was concentrated. The resulting crude product was chromatographed (silica, CH_2Cl_2) to afford unreacted porphyrin monomers followed by the desired dyad and then high molecular weight material (HMWM). The mixture of dyad and HMWM was concentrated to dryness, dissolved in THF, and chromatographed (SEC, THF) with gravity elution. The dyad-containing fractions were combined and chromatographed [silica, CH_2Cl_2/hexanes (1:1)] to afford a purple solid (33 mg, 47%): ^{1}H NMR (300 MHz, $CDCl_3$) δ −2.65 (br, 4H), 1.96 (s, 12H), 7.68−7.81 (m, 18H), 7.82 (s, 4H), 8.20 (s, 4H), 8.25 (dd, *J* = 7.8 Hz and 1.8 Hz, 8H), 8.77 (d, *J* = 4.8 Hz, 4H), 8.86 (s, 8H), 8.88 (d, *J* = 4.8 Hz, 4H); MALDI-MS obsd 1307.8, calcd exact mass 1306.5; λ_{abs} (CH_2Cl_2) 421, 512, 548 nm.

*1-[4-(5,10,15-Triphenylporphin-20-yl)-3,5-dimethylphenyl]-2-[4-(5,10,15-triphenylporphin-20-yl)phenyl]ethyne (**Fb$_2$-M**).* Following a copper-free procedure for Sonogashira coupling of porphyrins,[32,33] samples of **Fb-U** (31.9 mg, 50.0 μmol), **Fb-H-I** (38.4 mg, 50.0 μmol), and P(*o*-tol)$_3$ (18.2 mg, 60.0 μmol) in toluene/triethylamine [(5:1), 20 mL) were degassed by three freeze/pump/thaw cycles. Then $Pd_2(dba)_3$ (6.8 mg, 7.5 μmol) was added, and the mixture was additionally degassed by three freeze/pump/thaw cycles. The resulting mixture was stirred for 6 h at 40 °C in a Schlenk line. The reaction mixture was allowed to cool and then concentrated. The resulting crude product was chromatographed (silica, CH_2Cl_2) to afford unreacted porphyrin monomers followed by the desired dyad and then HMWM. The mixture of dyad and HMWM was concentrated to dryness, dissolved in THF, and chromatographed (SEC, THF) with gravity elution. The dyad-containing fractions were combined and chromatographed [silica, CH_2Cl_2/hexanes (1:1)] to afford a purple solid (26 mg, 41%): ^{1}H NMR (300 MHz, $CDCl_3$) δ −2.74 (br, 2H), −2.66 (br, 2H), 1.96 (s, 6H), 7.72−7.90 (m, 18H), 7.83 (s, 2H), 8.06 (d, *J* = 8.1 Hz, 2H), 8.18−8.26 (m, 12H), 8.29 (d, *J* = 8.1 Hz, 2H), 8.76 (d, *J* = 4.8 Hz, 2H), 8.82−8.88 (m, 10H), 8.89−8.96 (m, 4H); MALDI-MS obsd 1278.4, calcd exact mass 1278.5; λ_{abs} (CH_2Cl_2) 421, 515, 549 nm.

*Chloro{5,10,15-triphenyl-20-[2,6-dimethyl-4-ethynylphenyl]-porphinato}thallium(III) (**Tl-H**).* Following a reported procedure,[34] a solution of **Fb-H** (53.3 mg, 80.0 μmol) in CH_2Cl_2 (66 mL) was treated with $TlCl_3{\cdot}4H_2O$ (612 mg, 1.60 mmol) in CH_3OH (3 mL) at room temperature for 6 h. Then the reaction mixture was diluted with CH_2Cl_2 (25 mL) and washed with saturated aqueous $NaHCO_3$ and H_2O. The organic layer was separated, dried (Na_2SO_4), filtered, and concentrated to dryness under reduced pressure without any applied heat. Subsequent chromatography [silica, CH_2Cl_2/hexanes (1:1)] gave a green solid (38.3 mg, 53%): ^{1}H NMR (300 MHz, $CDCl_3$) δ 1.79 (s, 3H), 1.92 (s, 3H), 3.27 (s, 1H), 7.66 (d, *J*(H−H) = 6.6 Hz, 2H), 7.72−7.78 (m, 3H), 7.80−7.88 (m, 6H), 8.06−8.18 (m, 3H), 8.32−8.42 (m, 3H), 8.77 (d, *J*(H−H) = 4.8 Hz, 1H), 8.97 (d, *J*(H−H) = 4.8 Hz, 1H), 9.03 (d, *J*(Tl−H) = 63.6 Hz, 2H), 9.04 (d, *J*(Tl−H) = 66.0 Hz, 4H); MALDI-MS obsd 904.7; ESI-MS obsd 869.2359, calcd 869.2368 [$(\{M - Cl\}+ H)^+$, M = $C_{48}H_{32}ClN_4Tl$]; λ_{abs} (CH_2Cl_2) 433, 565, 607 nm.

*Chloro{5,10,15-triphenyl-20-[4-ethynylphenyl]porphinato}-thallium(III) (**Tl-U**).* Following a reported procedure,[34] a solution of **Fb-U** (21.7 mg, 34.0 μmol) in CH_2Cl_2 (28 mL) was treated with $TlCl_3{\cdot}4H_2O$ (260 mg, 680 μmol) in CH_3OH (1.5 mL) at room temperature for 6 h. Then the reaction mixture was diluted with CH_2Cl_2 (25 mL) and washed with saturated aqueous $NaHCO_3$ and H_2O. The organic layer was separated, dried (Na_2SO_4), filtered, and concentrated to dryness under reduced pressure without any heat. The resulting crude product was chromatographed [silica, CH_2Cl_2/hexanes (1:1)] to give a green solid (16.4 mg, 55%): ^{1}H NMR (300 MHz, $CDCl_3$) δ 3.33 (s, 1H), 7.70−7.86 (m, 9H), 7.92 (dd, *J*(H−H) = 17.6 Hz and 7.8 Hz, 2H), 8.12 (d, *J*(H−H) = 6.6 Hz, 4H), 8.30−8.42 (m, 4H), 9.03 (d, *J*(Tl−H) = 64.8 Hz, 2H), 9.04 (d, *J*(Tl−H) = 64.5 Hz, 2H), 9.06 (d, *J*(Tl−H) = 64.8 Hz, 2H), 9.08 (d, *J*(Tl−H) = 64.2 Hz, 2H); MALDI-MS obsd 876.5; ESI-MS obsd 839.2032, calcd 839.2027 [$(\{M - Cl\}+ H)^+$, M = $C_{46}H_{27}ClN_4Tl$]; λ_{abs}(CH_2Cl_2) 434, 566, 606 nm.

*Dichloro[1,2-bis[4-(5,10,15-triphenylporphinatothallium(III)-20-yl)-3,5-dimethylphenyl]ethyne] (**Tl$_2$-B**).* Following a reported procedure,[34] a solution of **Fb$_2$-B** (15.7 mg, 12.0 μmol) in CH_2Cl_2 (10 mL) was treated with $TlCl_3{\cdot}4H_2O$ (230 mg, 600 μmol) in CH_3OH (1 mL) at room temperature for 6 h. Then the reaction mixture was diluted with CH_2Cl_2 (25 mL) and washed with saturated aqueous $NaHCO_3$ and H_2O. The organic layer was separated, dried (Na_2SO_4), filtered, and concentrated to dryness under reduced pressure without any applied heat. Subsequent chromatography [silica, CH_2Cl_2/hexanes (1:1)] gave a green solid (12.4 mg, 58%): ^{1}H NMR (300 MHz, $CDCl_3$) δ 1.89 (s, 6H), 2.03 (s, 6H), 7.68−7.88 (m, 22H), 8.13 (dd, *J*(H−H) = 16.6 Hz and 7.5 Hz, 6H), 8.40 (d, *J*(H−H) = 3.3 Hz, 6H), 8.99 (dd, *J*(H−H), = 4.8 Hz, *J*(Tl−H) = 61.5 Hz, 4H), 9.06 (d, *J*(Tl−H) = 65.7 Hz, 8H), 9.09 (dd, *J*(H−H), = 4.8 Hz, *J*(Tl−H) = 63.0 Hz, 4H); MALDI-MS obsd 1786.6, calcd exact mass 1782.4; λ_{abs} (CH_2Cl_2) 436, 566, 606 nm.

*Dichloro[1-[4-(5,10,15-triphenylporphinatothallium(III)-20-yl)-3,5-dimethylphenyl]-2-[4-(5,10,15-triphenylporphinatothallium(III)-20-yl)phenyl]ethyne (**Tl$_2$-M**).* Following a reported procedure,[34] a solution of **Fb$_2$-M** (21.9 mg, 17.2 μmol) in CH_2Cl_2 (15 mL) was treated with $TlCl_3{\cdot}4H_2O$ (329 mg, 860 μmol) in CH_3OH (1.5 mL) at room temperature for 6 h. Then the reaction mixture was diluted with CH_2Cl_2 (25 mL) and washed with saturated aqueous $NaHCO_3$ and H_2O. The organic layer was separated, dried (Na_2SO_4), filtered, and concentrated to dryness under reduced pressure without any applied heat. Subsequent chromatography [silica, CH_2Cl_2/hexanes (1:1)] gave a green solid (18.7 mg, 62%): ^{1}H NMR (300 MHz, $CDCl_3$) δ 1.90 (s, 3H), 2.03 (s, 3H), 7.72−7.90 (m, 20H), 8.05−8.20 (m, 8H), 8.22 (d, *J*(H−H)= 8.1 Hz, 1H), 8.34−8.48 (m, 7H), 8.88 (d, *J*(H−H) = 5.4 Hz, 1H), 9.03 (q, *J*(H−H) = 4.8 Hz, 2H), 9.07 (dd, *J*(H−H) = 4.8 Hz and *J*(Tl−H) = 65.2 Hz, 8H), 9.08 (d, *J*(H−H) = 4.8 Hz, 1H), 9.10 (d, *J*(Tl−H) = 63.3 Hz, 2H), 9.25 (q, *J*(H−H) = 4.8 Hz, 2H); MALDI-MS obsd 1755.1, calcd exact mass 1754.4; λ_{abs} (CH_2Cl_2) 436, 567, 608 nm.

*Dichloro[1,2-bis[4-(5,10,15-triphenylporphinatothallium(III)-20-yl)phenyl]ethyne] (**Tl$_2$-U**).* Following a copper-free procedure for Sonogashira coupling of porphyrins,[32,33] samples of **Fb-U** (23.7 mg, 36.4 μmol), **Fb-U-I** (27.0 mg, 36.4 μmol), and P(*o*-tol)$_3$ (13.3 mg, 43.7 μmol) in toluene/triethylamine [(5:1), 15 mL) were degassed by three freeze/pump/thaw cycles. Then $Pd_2(dba)_3$ (5.0 mg, 5.5 μmol) was added, and the mixture was additionally degassed by three freeze/pump/thaw cycles. The resulting mixture was stirred for 6 h at 40 °C in a Schlenk line. The reaction mixture was allowed to cool and then concentrated. The resulting crude product was chromatographed (silica, CH_2Cl_2) to afford unreacted porphyrin monomers followed by the desired dyad and then HMWM. The mixture of dyad and HMWM was concentrated to dryness, dissolved in THF, and chromatographed (SEC, THF) with gravity elution. The dyad-containing fractions were combined and chromatographed [silica, CH_2Cl_2/hexanes (1:1)] to afford 1,2-bis[4-(5,10,15-triphenylporphin-20-yl)phenyl]ethyne (**Fb$_2$-U**) as a purple solid (12.8 mg, 28%) with the following characterization data: MALDI-MS obsd 1250.9, calcd exact mass 1250.5; λ_{abs} (CH_2Cl_2) 421, 516, 552 nm. Following a reported procedure,[34] a solution of **Fb$_2$-U** (10.7 mg, 8.6 μmol) in CH_2Cl_2 (7 mL) was treated with $TlCl_3{\cdot}4H_2O$ (431 mg, 431 μmol) in CH_3OH (0.7 mL) at room temperature for 6 h. Then the reaction mixture was diluted with CH_2Cl_2 (25 mL) and washed with saturated aqueous $NaHCO_3$ and H_2O. The organic layer was separated, dried (Na_2SO_4), filtered, and concentrated to dryness under reduced pressure without any heat. Subsequent chromatography [silica, CH_2Cl_2/hexanes (1:1)] gave a

dx.doi.org/10.1021/ic301613k | *Inorg. Chem.* XXXX, XXX, XXX−XXX

green solid (7.6 mg, 51%): ^{1}H NMR (300 MHz, $CDCl_3$) δ 7.71−7.90 (m, 18H), 8.09 (d, J(H−H) = 7.8 Hz, 2H), 8.15 (d, J(H−H) = 6.6 Hz, 8H), 8.23 (d, J(H−H) = 7.8 Hz, 2H), 8.32−8.42 (m, 6H), 8.46 (d, J(H−H) = 7.8 Hz, 2H), 9.03 (q, J(H−H) = 4.5 Hz, 4H), 9.08 (d, J(Tl−H) = 65.1 Hz, 8H), 9.25 (q, J(H−H) = 4.8 Hz, 4H); MALDI-MS obsd 1726.5, calcd exact mass 1726.3; λ_{abs} (CH_2Cl_2) 437, 567, 607 nm.

■ ASSOCIATED CONTENT

Supporting Information

Spectral data for all new compounds; EPR simulation parameters for the dyads. This material is available free of charge via the Internet at http://pubs.acs.org.

■ AUTHOR INFORMATION

Corresponding Author

*E-mail: holten@wustl.edu (D.H.), jlindsey@ncsu.edu (J.S.L.), david.bocian@ucr.edu (D.F.B.).

Notes

The authors declare no competing financial interest.

■ ACKNOWLEDGMENTS

This work was supported by a grant from the Chemical Sciences, Geosciences and Biosciences Division, Office of Basic Energy Sciences, of the U.S. Department of Energy to D.F.B. (DE-FG02-05ER15660), J.S.L. (DE-FG02-96ER14632), and D.H. (DE-FG02-05ER15661). Mass spectra were obtained at the Mass Spectrometry Laboratory for Biotechnology at North Carolina State University. Partial funding for the facility was obtained from the North Carolina Biotechnology Center and the National Science Foundation.

■ REFERENCES

(1) Maretina, I. A. *Russ. J. Gen. Chem.* **2009**, *79*, 1544−1581.
(2) Aratani, N.; Kim, D.; Osuka, A. *Acc. Chem. Res.* **2009**, *42*, 1922−1934.
(3) Flamigni, L. *J. Photochem. Photobiol., C* **2007**, *8*, 191−210.
(4) Nakamura, Y.; Aratani, N.; Osuka, A. *Chem. Soc. Rev.* **2007**, *36*, 831−845.
(5) Lo, P.-C.; Leng, X.; Ng, D. K. P. *Coord. Chem. Rev.* **2007**, *251*, 2334−2353.
(6) Kobuke, Y. *Struct. Bonding (Berlin)* **2006**, *121*, 49−104.
(7) Iengo, E.; Scandola, F.; Alessio, E. *Struct. Bonding (Berlin)* **2006**, *121*, 105−143.
(8) Balaban, T. S. *Acc. Chem. Res.* **2005**, *38*, 612−623.
(9) Balaban, T. S.; Tamiaki, H.; Holzwarth, A. R. *Top. Curr. Chem.* **2005**, *258*, 1−38.
(10) Imahori, H. *J. Phys. Chem. B* **2004**, *108*, 6130−6143.
(11) (a) Harvey, P. D. In *The Porphyrin Handbook*; Kadish, K. M., Smith, K. M., Guilard, R., Eds.; Academic Press: San Diego, CA, 2003; Vol. *18*, pp 63−250. (b) Harvey, P. D.; Stern, C.; Guilard, R. In *Handbook of Porphyrin Science*; Kadish, K. M., Smith, K. M., Guilard, R., Eds.; World Scientific Publishing Co.: Singapore, 2011; Vol. *11*, Ch. 49, pp 1−179.
(12) Aratani, N.; Osuka, A. *Chem. Rec.* **2003**, *3*, 225−234.
(13) Holten, D.; Bocian, D. F.; Lindsey, J. S. *Acc. Chem. Res.* **2002**, *35*, 57−69.
(14) Aratani, N.; Osuka, A. *Macromol. Rapid Commun.* **2001**, *22*, 725−740.
(15) Burrell, A. K.; Officer, D. L.; Plieger, P. G.; Reid, D. C. W. *Chem. Rev.* **2001**, *101*, 2751−2796.
(16) Gust, D.; Moore, T. A.; Moore, A. L. *Acc. Chem. Res.* **2001**, *34*, 40−48.
(17) Seth, J.; Palaniappan, V.; Johnson, T. E.; Prathapan, S.; Lindsey, J. S.; Bocian, D. F. *J. Am. Chem. Soc.* **1994**, *116*, 10578−10592.
(18) Seth, J.; Palaniappan, V.; Wagner, R. W.; Johnson, T. E.; Lindsey, J. S.; Bocian, D. F. *J. Am. Chem. Soc.* **1996**, *118*, 11194−11207.
(19) Yang, S. I.; Lammi, R. K.; Seth, J.; Riggs, J. A.; Arai, T.; Kim, D.; Bocian, D. F.; Holten, D.; Lindsey, J. S. *J. Phys. Chem. B* **1998**, *102*, 9426−9436.
(20) Thamyongkit, P.; Muresan, A. Z.; Diers, J. R.; Holten, D.; Bocian, D. F.; Lindsey, J. S. *J. Org. Chem.* **2007**, *72*, 5207−5217.
(21) Muresan, A, Z.; Thamyongkit, P.; Diers, J. R.; Holten, D.; Lindsey, J. S.; Bocian, D. F. *J. Org. Chem.* **2008**, *73*, 6947−6959.
(22) Nieves-Bernier, E. J.; Diers, J. R.; Taniguchi, M.; Holten, D.; Bocian, D. F.; Lindsey, J. S. *J. Org. Chem.* **2010**, *75*, 3193−3202.
(23) Diers, J. R.; Taniguchi, M.; Holten, D.; Lindsey, J. S.; Bocian, D. F. *J. Am. Chem. Soc.* **2010**, *132*, 12121−12132.
(24) Wagner, R. W.; Johnson, T. E.; Lindsey, J. S. *J. Am. Chem. Soc.* **1996**, *118*, 11166−11180.
(25) Rochford, J.; Galoppini, E. *Langmuir* **2008**, *24*, 5366−5374.
(26) Cohen, B. W.; Lovaasen, B. M.; Simpson, C. K.; Cummings, S. D.; Dallinger, R. F.; Hopkins, M. D. *Inorg. Chem.* **2010**, *49*, 5777−5779.
(27) Baker, G. A.; Bright, F. V.; Detty, M. R.; Pandey, S.; Stilts, C. E.; Yao, H. *J. Porphyrins Phthalocyanines* **2000**, *4*, 669−683.
(28) Zaidi, S. H. H.; Fico, R. M., Jr.; Lindsey, J. S. *Org. Process Res. Dev.* **2006**, *10*, 118−134.
(29) Tamaru, S.-I.; Yu, L.; Youngblood, W. J.; Muthukumaran, K.; Taniguchi, M.; Lindsey, J. S. *J. Org. Chem.* **2004**, *69*, 765−777.
(30) Lindsey, J. S. *Acc. Chem. Res.* **2010**, *43*, 300−311.
(31) Unterlass, M. M.; Espinosa, E.; Boisson, F.; D'Agosto, F.; Boisson, C.; Ariga, K.; Khalakhan, I.; Charvet, R.; Hill, J. P. *Chem. Commun.* **2011**, *47*, 7057−7059.
(32) Wagner, R. W.; Johnson, T. E.; Li, F.; Lindsey, J. S. *J. Org. Chem.* **1995**, *60*, 5266−5273.
(33) Wagner, R. W.; Ciringh, Y.; Clausen, C.; Lindsey, J. S. *Chem. Mater.* **1999**, *11*, 2974−2983.
(34) Taniguchi, M.; Lindsey, J. S. *Tetrahedron* **2010**, *66*, 5549−5565.
(35) (a) Marcus, R. A.; Sutin, N. *Biochim. Biophys. Acta* **1985**, *811*, 265−322. (b) Nitzan, A. *Chemical Dynamics in Condensed Phases: Relaxation, Transfer, and Reactions in Condensed Molecular Systems*; Oxford University Press: New York, 2006.
(36) (a) Eaton, S. S.; Eaton, G. R. *J. Am. Chem. Soc.* **1975**, *97*, 3660−3666. (b) Eaton, S. S.; Eaton, G. R. *J. Am. Chem. Soc.* **1977**, *99*, 6594−6599.
(37) (a) Song, H.-E.; Kirmaier, C.; Diers, J. R.; Lindsey, J. S.; Bocian, D. F.; Holten, D. *J. Phys. Chem. B* **2009**, *113*, 54−63. (b) Song, H.-E.; Taniguchi, M.; Diers, J. R.; Kirmaier, C.; Bocian, D. F.; Lindsey, J. S.; Holten, D. *J. Phys. Chem. B* **2009**, *113*, 16483−16493. (c) Song, H.-E.; Kirmaier, C.; Taniguchi, M.; Diers, J. R.; Bocian, D. F.; Lindsey, J. S.; Holten, D. *J. Am. Chem. Soc.* **2008**, *130*, 15636−15648.
(38) Srinivasan, N.; Haney, C. A.; Lindsey, J. S.; Zhang, W.; Chait, B. T. *J. Porphyrins Phthalocyanines* **1999**, *3*, 283−291.
(39) del Rosario Benites, M.; Johnson, T. E.; Weghorn, S.; Yu, L.; Rao, P. D.; Diers, J. R.; Yang, S. I.; Kirmaier, C.; Bocian, D. F.; Holten, D.; Lindsey, J. S. *J. Mater. Chem.* **2002**, *12*, 65−80.
(40) Lindsey, J. S.; Prathapan, S.; Johnson, T. E.; Wagner, R. W. *Tetrahedron* **1994**, *50*, 8941−8968.
(41) Laha, J. K.; Dhanalekshmi, S.; Taniguchi, M.; Ambroise, A.; Lindsey, J. S. *Org. Process Res. Dev.* **2003**, *7*, 799−812.
(42) Thamyongkit, P.; Lindsey, J. S. *J. Org. Chem.* **2004**, *69*, 5796−5799.
(43) Yang, S. I.; Seth, J.; Strachan, J.-P.; Gentemann, S.; Kim, D.; Holten, D.; Lindsey, J. S.; Bocian, D. F. *J. Porphyrins Phthalocyanines* **1999**, *3*, 117−147.
(44) (a) Duling, D. R. *J. Magn. Reson. B* **1994**, *104*, 105−110. (b) http://www.niehs.nih.gov/research/resources/software/tools/index.cfm (accession date 03/18/2010).
(45) Heinzer, J. *Mol. Phys.* **1971**, *22*, 167−177.
(46) Heinzer, J. *Quantum Chemistry Program Exchange, No. 209*, 1972.

(47) Except for molecular mechanics and semi-empirical models, the calculation methods used in Spartan '08 or '10 have been documented in: Shao, Y.; Molnar, L. F.; Jung, Y.; Kussmann, J.; Ochsenfeld, C.; Brown, S. T.; Gilbert, A. T. B.; Slipchenko, L. V.; Levchenko, S. V.; O'Neill, D. P.; DiStasio, R. A., Jr.; Lochan, R. C.; Wang, T.; Beran, G. J. O.; Besley, N. A.; Herbert, J. M.; Lin, C. Y.; Van Voorhis, T.; Chien, S. H.; Sodt, A.; Steele, R. P.; Rassolov, V. A.; Maslen, P. E.; Korambath, P. P.; Adamson, R. D.; Austin, B.; Baker, J.; Byrd, E. F. C.; Dachsel, H.; Doerksen, R. J.; Dreuw, A.; Dunietz, B. D.; Dutoi, A. D.; Furlani, T. R.; Gwaltney, S. R.; Heyden, A.; Hirata, S.; Hsu, C.-P.; Kedziora, G.; Khalliulin, R. Z.; Klunzinger, P.; Lee, A. M.; Lee, M. S.; Liang, W.-Z.; Lotan, I.; Nair, N.; Peters, B.; Proynov, E. I.; Pieniazek, P. A.; Rhee, Y. M.; Ritchie, J.; Rosta, E.; Sherrill, C. D.; Simmonett, A. C.; Subotnik, J. E.; Woodcock, H. L., III; Zhang, W.; Bell, A. T.; Chakraborty, A. K.; Chipman, D. M.; Keil, F. J.; Warshel, A.; Hehre, W. J.; Schaefer, H. F., III; Kong, J.; Krylov, A. I.; Gill, P. M. W.; Head-Gordon, M. *Phys. Chem. Chem. Phys.* **2006**, *8*, 3172−3191.

dx.doi.org/10.1021/ic301613k | *Inorg. Chem.* XXXX, XXX, XXX−XXX